The symmetry energy γ parameter of relativistic mean-field models *

Mariana Dutra[1] Odilon Lourenço[2] Or Hen[3] Eliezer Piasetzky[4] Débora P. Menezes[5]

[1] Departamento de Ciências da Natureza, Universidade Federal Fluminense, 28895-532, Rio das Ostras, RJ, Brazil
[2] Universidade Federal do Rio de Janeiro, 27930-560, Macaé, RJ, Brazil
[3] Massachusetts Institute of Technology, Cambridge, Massachusetts 02139, USA
[4] School of Physics and Astronomy, Tel Aviv University, Tel Aviv 69978, Israel
[5] Depto de Física - CFM - Universidade Federal de Santa Catarina, Florianópolis - SC - CP. 476 - CEP 88.040-900, Brazil

Abstract: The relativistic mean-field models tested in previous works against nuclear matter experimental values, critical parameters and macroscopic stellar properties are revisited and used in the evaluation of the symmetry energy γ parameter obtained in three different ways. We have checked that, independent of the choice made to calculate the γ values, a trend of linear correlation is observed between γ and the symmetry energy ($\mathcal{S}_0$) and a more clear linear relationship is established between γ and the slope of the symmetry energy (L_0). These results directly contribute to the arising of other linear correlations between γ and the neutron star radii of $R_{1.0}$ and $R_{1.4}$, in agreement with recent findings. Finally, we have found that short-range correlations induce two specific parametrizations, namely, IU-FSU and DD-MEδ, simultaneously compatible with the neutron star mass constraint of $1.93\leqslant M_{\rm max}/M_\odot\leqslant 2.05$ and with the overlap band for the $L_0\times\mathcal{S}_0$ region, to present γ in the range of $\gamma=0.25\pm0.05$.

Keywords: symmetry energy, relativistic mean-field models, nuclear matter

PACS: 21.65.Ef, 24.10.Jv, 21.65.Mn **DOI:** 10.1088/1674-1137/42/6/064105

1 Introduction

Since the introduction of the first models in nuclear physics, the main idea was to describe experimental data. Not all nuclear models can be applied to the description of nuclear matter but they are relevant nevertheless. Relativistic mean field (RMF) models were developed to describe observables of nuclei, from which nuclear matter parameters can be extracted.

A detailed analysis of 263 RMF models based on pure neutron and symmetric nuclear matter properties was done in Ref. [1], and only 35 of them were shown to satisfy important nuclear constraints. In a subsequent work, these models were used to analyse stellar properties related to commonly studied astrophysical quantities, namely, neutron star masses and radii of the canonical neutron stars (obtained from observational data), the possible onset of the Direct Urca process and sound velocity constraints [2]. As a result, only 13 out of them produced neutron stars with maximum mass in the range of $1.93\leqslant M_{\rm max}/M_\odot\leqslant 2.05$ [3, 4] without considering hyperons, including one with density-dependent couplings (DD-F) and one also incorporating scalar-isovector δ mesons (DD-MEδ). The remaining parametrizations (BKA20, BKA22, BKA24, BSR8, BSR9, BSR10, BSR11, BSR12, FSUGZ03, IU-FSU, G2*) present constant couplings, non-linear σ and ω terms, and cross terms involving these fields. None of them could reproduce pulsars with $2M_\odot$ if hyperons were included. More recently, the same models were revisited and their critical parameters were obtained [5]. These critical parameters are the critical temperature, critical pressure and critical density, at which nuclear matter is no longer unstable and the liquid-gas phase transition ceases to exist [6–12]. In this investigation, the models were divided into 6 categories (BKA, BSR, FSU, G2*, Z271 and DD). More experimental data is necessary, but so far, only two of them (Z271 and DD) provided critical temperatures close to existing ones. A clear correlation between the critical temperature and the compressibility was obtained. More details of these models are given later in this paper.

In the same context, the symmetry energy [13] and its slope are very important quantities and in the last fifteen years, they were shown to be correlated with a series of physical properties, on which we comment next. The

Received 10 November 2017, Revised 2 April 2018, Published online 4 May 2018

∗ This work is a part of the project INCT-FNA Proc. No. 464898/2014-5 and was partially supported by Conselho Nacional de Desenvolvimento Científico e Tecnológico (CNPq), Brazil under grants 300602/2009-0 and 306786/2014-1. E. P. acknowledges support from the Israel Science Foundation. O. H. acknowledges the U.S. Department of Energy Office of Science, Office of Nuclear Physics program under award number DE-FG02-94ER40818

1) E-mail: marianadutra@id.uff.br

symmetry energy is related to the nuclei neutron skin thickness, which in turn is related to neutron star radius: models that yield smaller neutron skin thickness in heavy nuclei, give rise to smaller neutron star radii [14]. On the other hand, neutron skins are larger for models with higher slope [15]. Also, a strong correlation has been observed between the neutron star radius and the variation of the slope at sub-threshold densities [16]. The symmetry energy and the slope, however, can be easily controlled by the inclusion of a $\omega-\rho$ [15, 17–19] or a $\sigma-\rho$ interaction [20] in non-linear models. The larger the value of the $\omega-\rho$ interaction, for instance, the lower the values of the symmetry energy and its slope. On the other hand, for density-dependent models a change in the density dependence of the ρ-meson coupling can modify the symmetry energy and its slope.

Besides the neutron skin thickness, the neutron star crust-core properties are also correlated with the slope of the symmetry energy, a fact that had already been observed in studies involving liquid-gas phase transitions, whose transition densities are approximately the same as those obtained as the separating densities from the pasta phase to homogeneous matter [21].

We next reanalyze the parametrizations studied in Ref. [1], which we call *consistent relativistic mean field* (CRMF) models from now on. In this context, the word "consistent" refers to those parametrizations that were shown to satisfy the nuclear matter constraints in Ref. [1]. For these CRMF parametrizations, we evaluate the symmetry energy coefficient γ in three different cases. Such a quantity is defined from $\mathcal{S}=\mathcal{S}^{\rm kin}+\mathcal{S}^{\rm pot}$, with $\mathcal{S}^{\rm pot}(\rho)\propto(\rho/\rho_0)^{\gamma}$ and was first analyzed in Refs. [22, 23]. Our aim is to look for possible correlations between the γ parameter and some important nuclear matter and neutron star properties, namely the symmetry energy, its slope, and the radii of 1.0 and 1.4 solar mass neutron stars. Within the assumptions made in the present work, the γ parameter fully defines the potential part of the symmetry energy and its density dependence. Theoretically, γ is sensitive to the nucleon-nucleon interaction at very short distances and can be extracted from the existing calculations. We also investigate which parametrizations satisfy the ranges of γ recently obtained in Refs. [24, 25]. It is worth pointing out that from the experimental side, the γ parameter is not directly measured but, as for most of the bulk nuclear matter properties, it can be inferred from experiments. In order to be consistent with previous studies, the $\omega-\rho$ and $\sigma-\rho$ interactions that can be included in most models to *cure* their symmetry energy and slope values are left aside. They are just considered in the models that introduced them when they were proposed.

The rest of this paper is organized as follows. In Section 2, the formalism is introduced and three different forms of separate kinetic and potential parts of the symmetry energy are presented. In Section 3 the results are discussed. A summary is given in Section 4.

2 Formalism

The analysis performed in Ref. [1] pointed to only 35 parametrizations, out of the 263 investigated, that simultaneously meet seven distinct nuclear matter constraints. These CRMF parametrizations had their bulk and thermodynamical quantities compared to respective theoretical/experimental data from symmetric nuclear matter (SNM), pure neutron matter (PNM), and a mixture of both, namely, symmetry energy and its slope evaluated at the saturation density, and the ratio of the symmetry energy at $\rho_0/2$ to its value at ρ_0 (MIX). These detailed constraints are specified in Table 1.

Table 1. Set of updated constraints (SET2a) used in Ref. [1]. See that reference for more details.

constraint	quantity	density region	range
SM1	K_0	at ρ_0	190 − 270 MeV
SM3a	$P(\rho)$	$2<\frac{\rho}{\rho_0}<5$	band region
SM4	$P(\rho)$	$1.2<\frac{\rho}{\rho_0}<2.2$	band region
PNM1	$\mathcal{E}_{\rm PNM}/\rho$	$0.017<\frac{\rho}{\rho_{\rm o}}<0.108$	band region
MIX1a	J	at ρ_0	25 − 35 MeV
MIX2a	L_0	at ρ_0	25 − 115 MeV
MIX4	$\frac{\mathcal{S}(\rho_0/2)}{J}$	at ρ_0 and $\rho_0/2$	0.57 − 0.86

In Table 2 we present a brief compilation of the structure and methods used in fitting the finite range RMF interactions in accordance with the macroscopic constraints, and the data used for the fittings. For full explanation and details, we refer readers to the original papers and for a complete description of the relativistic mean-field theory, to Ref. [26].

Thirty out of the 35 parametrizations which match the constraints analyzed in Ref. [1] are of type 4, i.e., the Lagrangian density includes non-linear σ and ω terms and cross terms involving these fields. They are: BKA20, BKA22, BKA24, BSR8, BSR9, BSR10, BSR11, BSR12, BSR15, BSR16, BSR17, BSR18, BSR19, BSR20, FSU-III, FSU-IV, FSUGold, FSUGold4, FSUGZ03, FSUGZ06, G2*, IU-FSU, Z271s2, Z271s3, Z271s4, Z271s5, Z271s6, Z271v4, Z271v5, and Z271v6. They are described by the following Lagrangian density,

Table 2. Structure of the RMF models and data used for fitting the finite range parametrizations considered in the present work. NL: non-linear model. DD: density dependent model. NAP: number of adjusted parameters. AT: additional terms in comparison with the standard non-linear $\sigma^3-\sigma^4$ model with meson ρ included.

parametrization	type of model, no. of parameters, NAP, AT	data used for fitting purposes
BKA20, BKA22, BKA24 [27]	NL, 12, 10 AT: ω^2, $\sigma-\omega^2$, $\sigma^2-\omega^2$, $\sigma-\rho^2$	Constraint properties of asymmetric nuclear matter for 26 different parametrizations: binding energies, charge radii for closed shell nuclei, neutron-skin thickness in the ^{208}Pb nucleus: 0.20, 0.22, and 0.24 fm.
BSR8 to BSR12 [28]	NL, 14, 11 AT: ω^2, $\sigma-\omega^2$, $\sigma^2-\omega^2$, $\sigma-\rho^2$, $\sigma^2-\rho^2$, $\omega^2-\rho^2$	Binding energies: ^{16,24}O, ^{40,48}Ca, ^{56,78}Ni, ^{88}Sr, ^{90}Zr,^{100,116,132}Sn, and ^{208}Pb nuclei, charge radii: ^{16}O, ^{40,48}Ca, ^{56}Ni, ^{88}Sr, ^{90}Zr, ^{116}Sn, and ^{208}Pb nuclei neutron skin thickness: ^{208}Pb free parameters: neutron-skin thickness ΔR=0.16,0.18,$\cdots$,0.28 fm and the ω-meson self-coupling strength ξ_0=0.03
BSR15 to BSR20 [28]	NL, 14, 11 AT: ω^2, $\sigma-\omega^2$, $\sigma^2-\omega^2$, $\sigma-\rho^2$, $\sigma^2-\rho^2$, $\omega^2-\rho^2$	The same as BSR8-BSR12 with ξ_0=0.06
FSU-III, FSU-IV[29]	NL, 10,7 AT: ω^2, $\omega^2-\rho^2$	Properties of asymmetric nuclear matter; the proton fraction in β-stable $npe\mu$ matter; the core-crust transition density and pressure in neutron stars as predicted by FSUGold and IU-FSU; free parameters: the coupling constants between the isovector ρ meson ($\Lambda_{\rm v}$) and the isoscalar σ and ω mesons ($\Lambda_{\rm s}$): FSU-III: $\Lambda_{\rm v}$=0.00 and $\Lambda_{\rm s}$=0.02 FSU-IV: $\Lambda_{\rm v}$=0.00 and $\Lambda_{\rm s}$=0.04
FSUGold [30]	NL, 10, 8 AT: ω^2, $\omega^2-\rho^2$	Binding energies and charge radii magic nuclei for ^{40}Ca, ^{90}Zr, ^{116,132}Sn, ^{208}Pb
FSUGold4 [31]	NL, 10, 8, AT: ω^2, $\omega^2-\rho^2$	Adjusting the isovector parameters of the model g_ρ and $\Lambda_{\rm v}$
FSUGZ03, FSUGZ06 [32]	NL, 14, 12 AT: ω^2, $\sigma-\omega^2$, $\sigma^2-\omega^2$, $\sigma-\rho^2$, $\sigma^2-\rho^2$, $\omega^2-\rho^2$	Binding energies: ^{16,24}O, ^{40,48}Ca, ^{56,78} Ni, ^{88}Sr, ^{90}Zr, ^{100,116,132}Sn,^{208}Pb charge rms radii:^{16}O, ^{40,48}Ca, ^{56} Ni, ^{88}Sr, ^{90}Zr, ^{116}Sn,^{208}Pb neutron-skin thickness for^{208}Pb nucleus: 0.18±0.01 fm free parameters: ζ and ξ corresponding to self-couplings for ω and ρ mesons: ζ=0.03,0.06 and ξ=0
G2* [33]	NL, 12, 10 AT: ω^2, $\sigma-\omega^2$, $\sigma^2-\omega^2$, $\sigma-\rho^2$	Adjust the isovector-vector channel of the G2 parameter set.
IU-FSU [34]	NL, 10, 10 AT: ω^2, $\omega^2-\rho^2$	Change the isoscalar parameter to ξ=0.03; refitting of the isoscalar parameters to maintain the saturation properties of SNM of FSU; increase the isoscalar-isovector coupling constant to Λ=0.046
Z271s2 to Z271s5 [35]	NL, 10, 8 AT: ω^2, $\sigma^2-\rho^2$	Model parameters used: Z271 free parameters: $\lambda_{\rm v}$=0 and $\lambda_{\rm s}$=0.020,0.030,0.040,0.050
Z271v4 to Z271v6 [35]	NL, 10, 8 AT: ω^2, $\omega^2-\rho^2$	The same as Z271s2-s5, but the free parameters are: $\lambda_{\rm s}$=0 and $\lambda_{\rm v}$=0.020,0.25,0.030
DD-F [36]	DD, 15, 12	Properties of finite nuclei: binding energies, charge and diffraction radii, surface thicknesses, neutron skin in ^{208}Pb, spin-orbit splittings
TW99 [37]	DD, 15, 12	Fix the density dependence of the couplings from Dirac-Brueckner calculations of nuclear matter binding energies of symmetric nuclei (^{16}O, ^{40}Ca, ^{56}Ni) and neutron-rich nuclei (^{24}O, ^{48}Ca, ^{90}Zr, ^{208}Pb).
DDHδ [38]	DD, 20, 16	Reproduce bulk asymmetry parameter a_4=33.4 MeV
DD-MEδ [39]	DD, 24, 14	Finite nuclei and adjustment to ab initio calculations in infinite nuclear matter

$$\begin{aligned}\mathcal{L}_{\rm NL} &= \overline{\psi}(i\gamma^\mu\partial_\mu - M)\psi + g_\sigma\sigma\overline{\psi}\psi - g_\omega\overline{\psi}\gamma^\mu\omega_\mu\psi - \frac{g_\rho}{2}\overline{\psi}\gamma^\mu\vec{\rho}_\mu\vec{\tau}\psi + \frac{1}{2}(\partial^\mu\sigma\partial_\mu\sigma - m_\sigma^2\sigma^2) - \frac{A}{3}\sigma^3 \\ &- \frac{B}{4}\sigma^4 - \frac{1}{4}F^{\mu\nu}F_{\mu\nu} + \frac{1}{2}m_\omega^2\omega_\mu\omega^\mu + \frac{C}{4}(g_\omega^2\omega_\mu\omega^\mu)^2 - \frac{1}{4}\vec{B}^{\mu\nu}\vec{B}_{\mu\nu} + \frac{1}{2}m_\rho^2\vec{\rho}_\mu\vec{\rho}^\mu + \frac{1}{2}\alpha_3' g_\omega^2 g_\rho^2\omega_\mu\omega^\mu\vec{\rho}_\mu\vec{\rho}^\mu \\ &+ g_\sigma g_\omega^2\sigma\omega_\mu\omega^\mu\left(\alpha_1 + \frac{1}{2}\alpha_1' g_\sigma\sigma\right) + g_\sigma g_\rho^2\sigma\vec{\rho}_\mu\vec{\rho}^\mu\left(\alpha_2 + \frac{1}{2}\alpha_2' g_\sigma\sigma\right), \end{aligned} \tag{1}$$

where $F_{\mu\nu}=\partial_\nu\omega_\mu-\partial_\mu\omega_\nu$ and $\vec{B}_{\mu\nu}=\partial_\nu\vec{\rho}_\mu-\partial_\mu\vec{\rho}_\nu$. The nucleon rest mass is M and the meson masses are $m_{\rm j}$, for ${\rm j}=\sigma,\omega$, and ρ.

The other four CRMF parametrizations are density-dependent (DD): DD-F, TW99, DDHδ and DD-MEδ. Their Lagrangian density reads:

$$\begin{aligned}\mathcal{L}_{\rm DD} &= \overline{\psi}(i\gamma^\mu\partial_\mu - M)\psi + \Gamma_\sigma(\rho)\sigma\overline{\psi}\psi - \Gamma_\omega(\rho)\overline{\psi}\gamma^\mu\omega_\mu\psi \\ &- \frac{\Gamma_\rho(\rho)}{2}\overline{\psi}\gamma^\mu\vec{\rho}_\mu\vec{\tau}\psi + \Gamma_\delta(\rho)\overline{\psi}\vec{\delta}\vec{\tau}\psi - \frac{1}{4}F^{\mu\nu}F_{\mu\nu} \\ &+ \frac{1}{2}(\partial^\mu\sigma\partial_\mu\sigma - m_\sigma^2\sigma^2) + \frac{1}{2}m_\omega^2\omega_\mu\omega^\mu - \frac{1}{4}\vec{B}^{\mu\nu}\vec{B}_{\mu\nu} \\ &+ \frac{1}{2}m_\rho^2\vec{\rho}_\mu\vec{\rho}^\mu + \frac{1}{2}(\partial^\mu\vec{\delta}\partial_\mu\vec{\delta} - m_\delta^2\vec{\delta}^2), \end{aligned} \tag{2}$$

where

$$\Gamma_{\rm i}(\rho) = \Gamma_{\rm i}(\rho_0)f_{\rm i}(x); \quad f_{\rm i}(x)=a_{\rm i}\frac{1+b_{\rm i}(x+d_{\rm i})^2}{1+c_{\rm i}(x+e_{\rm i})^2}, \tag{3}$$

for $i=\sigma,\omega$, and $x=\rho/\rho_0$. For the ρ coupling one has

$$\Gamma_\rho(\rho)=\Gamma_\rho(\rho_0){\rm e}^{-a_\rho(x-1)}. \tag{4}$$

The Lagrangian density describing the DD-F and TW99 parametrizations is the same as the one in Eq. (2) when the meson δ is not taken into account. For the DD-MEδ parametrization, the couplings in Eq. (3) are valid for ${\rm i}=\sigma,\omega,\rho$, and δ. Finally, the DDHδ model has the same coupling parameters as in Eq. (3) for the mesons σ and ω, but functions $f_{\rm i}(x)$ given by

$$f_{\rm i}(x)=a_{\rm i}{\rm e}^{-b_{\rm i}(x-1)}-c_{\rm i}(x-d_{\rm i}), \tag{5}$$

for ${\rm i}=\rho,\delta$.

Only one parametrization belongs to the non-linear point coupling category, namely, the FA3 [40]. In this kind of model, nucleons interact with each other without explicitly including mesons [41–44]. Here, we do not investigate such a model since in Ref [2] we have shown it is not capable of generating a mass radius curve for neutron stars, due to a very particular behavior in the high-density regime, namely, a fall in the pressure versus energy density ($\mathcal{E}$) curve near $\mathcal{E}=809$ MeV/fm^3. For that reason, we have decided to discard this particular parametrization.

All the details about the RMF approximation and related equations of state (EoS) are given in Ref. [1] and will not be repeated here. Only the formulae necessary for the understanding of the present analysis are defined next.

The general definition of the symmetry energy reads as follows,

$$\mathcal{S}(\rho) = \frac{1}{8}\frac{\partial^2(\mathcal{E}/\rho)}{\partial y^2}\bigg|_{\rho,y=1/2} = \mathcal{S}^{kin}(\rho)+\mathcal{S}^{\rm pot}(\rho), \tag{6}$$

where $y=\rho_{\rm p}/\rho$ is the proton fraction of the system with $\rho_{\rm p}$ being the proton density. By using such an expression, we compute the kinetic and potential contributions of the symmetry energy slope

$$\begin{aligned} L(\rho) &= 3\rho\frac{\partial\mathcal{S}}{\partial\rho} = 3\rho\frac{\partial\mathcal{S}^{\rm kin}}{\partial\rho} + 3\rho\frac{\partial\mathcal{S}^{\rm pot}}{\partial\rho} \\ &= L^{\rm kin}(\rho)+L^{\rm pot}(\rho). \end{aligned} \tag{7}$$

If we consider the potential part of the symmetry energy written as a power-law in density according to

$$\mathcal{S}^{\rm pot}(\rho)=\mathcal{S}_0^{\rm pot}(\rho/\rho_0)^\gamma \equiv S_{\rm approx.}^{\rm pot}(\rho), \tag{8}$$

it is possible to express L_0 as

$$L_0=3\rho_0\left[\left(\frac{\partial\mathcal{S}^{\rm kin}}{\partial\rho}\right)_{\rho=\rho_0}+\frac{\gamma}{\rho_0}\mathcal{S}_0^{\rm pot}\right]. \tag{9}$$

By using Eq. (7) at $\rho=\rho_0$ and comparing it to Eq. (9), one can find γ as in Ref. [24], namely,

$$\gamma=\frac{L_0-L_0^{\rm kin}}{3\mathcal{S}_0^{\rm pot}}=\frac{L_0^{\rm pot}}{3\mathcal{S}_0^{\rm pot}}, \tag{10}$$

where $\mathcal{F}_0^{\rm kin,pot}=\mathcal{F}^{\rm kin,pot}(\rho_0)$, for $\mathcal{F}=\mathcal{S}$, L. In Ref. [24], the authors also introduced effects from short-range correlations (SRC) between proton-neutron pairs [45–47] in symmetric nuclear matter in order to provide an analytical expression for the kinetic part of the symmetry energy. From this expression, which we will also use in Section 2.3, they found the range of -10 ± 7.5 MeV for the kinetic part of the symmetry energy at the saturation density, $\mathcal{S}_0^{\rm kin}$, based on data from free proton-to-neutron ratios measured in intermediate energy nucleus-nucleus collisions. Such a range allowed the authors to predict the values of $\gamma=0.25\pm0.05$.

Another proposition for the calculation of the γ value is given in Ref. [25], where no short-range correlations in the kinetic part of the symmetry energy are taken into account. In that case, the density dependence of the symmetry energy was given by

$$\mathcal{S}(\rho)=\mathcal{S}^{\rm kin}(\rho)+\mathcal{S}^{\rm pot}(\rho)=a(\rho/\rho_0)^{2/3}+b(\rho/\rho_0)^\gamma, \tag{11}$$

with $a=12$ MeV, $b=22$ MeV, and γ possibly ranging from 0.5 to 1.5 corresponding respectively to a soft and

a stiff dependence. In that paper [25], a constraint for the nuclear symmetry energy at suprasaturation densities was deduced from the ASY-EOS experiment at GSI at twice saturation density, where the measurement of the elliptic flows of neutrons and light-charged particles in a gold-gold reaction resulted in γ=0.72±0.19.

2.1 Complete kinetic term (case 1)

Here we consider the *complete* kinetic term for the different models. Within this assumption, the first term of the symmetry energy is the kinetic part and the remaining is treated as the potential part. For the kinetic part, the corresponding expressions for non-linear and density-dependent (with δ meson) RMF models are,

$$\mathcal{S}_{\rm i}^{\rm kin}(\rho) = \frac{k_{\rm F}^2}{6E_{\rm Fi}^*} \tag{12}$$

where i= NL, DD, with $E_{\rm Fi}^*=(k_{\rm F}^2+M_{\rm i}^{*2})^{1/2}$ and

$$M_{\rm NL}^*=M-g_\sigma\sigma, \quad M_{\rm DD}^*=M-\Gamma_\sigma(\rho)\sigma, \tag{13}$$

for symmetric matter ($y=1/2$). The Fermi momentum is written in term of density as $k_{\rm F}=(3\pi^2\rho/2)^{1/3}$.

The potential part of the symmetry energy is written as

$$\mathcal{S}_{\rm NL}^{\rm pot}(\rho) = \frac{g_\rho^2}{8m_\rho^{*2}}\rho, \tag{14}$$

$$\mathcal{S}_{\rm DD}^{\rm pot}(\rho) = \frac{\Gamma_\rho^2\rho}{8m_\rho^2}-\frac{(\Gamma_\delta/m_\delta)^2(M_{\rm DD}^*)^2\rho}{2E_{\rm F\,DD}^{*2}\left[1+\left(\frac{\Gamma_\delta}{m_\delta}\right)^2 A_{\rm DD}\right]}, \tag{15}$$

where

$$m_\rho^{*2} = m_\rho^2+g_\sigma g_\rho^2\sigma(2\alpha_2+\alpha_2' g_\sigma\sigma)+\alpha_3' g_\omega^2 g_\rho^2\omega_0^2, \text{ and} \tag{16}$$

$$A_{\rm DD} = \frac{2}{\pi^2}\int_0^{k_{\rm F}}\frac{k^4{\rm d}k}{[k^2+(M_{\rm DD}^*)^2]^{3/2}}=3\left(\frac{\rho_{\rm s}}{M_{\rm DD}^*}-\frac{\rho}{E_{\rm F\,DD}^*}\right). \tag{17}$$

The mean-field value of the vector field ω_μ is ω_0, and $\rho_{\rm s}$ is the scalar density.

The respective expressions for the different contributions of the symmetry energy slope, namely, $L^{\rm kin}(\rho)$ and $L^{\rm pot}(\rho)$, are obtained as indicated in Eq. (7), for this case and the next ones.

2.2 "Free" kinetic term (case 2)

In this case we have separated the *really kinetic term*, the one without any dependence of the interaction with the mesons, from the rest of the symmetry energy. The expressions in this case read

$$\mathcal{S}_{\rm NL}^{\rm kin}(\rho)=\mathcal{S}_{\rm DD}^{\rm kin}(\rho)=\frac{k_{\rm F}^2}{6E_{\rm F}}, \tag{18}$$

with $E_{\rm F}=(k_{\rm F}^2+M^2)^{1/2}$, for the kinetic part, and

$$\mathcal{S}_{\rm NL}^{\rm pot}(\rho) = \frac{k_{\rm F}^2}{6E_{\rm F\,NL}^*}-\frac{k_{\rm F}^2}{6E_{\rm F}}+\frac{g_\rho^2}{8m_\rho^{*2}}\rho, \tag{19}$$

$$\mathcal{S}_{\rm DD}^{\rm pot}(\rho) = \frac{k_{\rm F}^2}{6E_{\rm F\,DD}^*}-\frac{k_{\rm F}^2}{6E_{\rm F}}+\frac{\Gamma_\rho^2\rho}{8m_\rho^2} -\frac{(\Gamma_\delta/m_\delta)^2(M_{\rm DD}^*)^2\rho}{2E_{\rm F\,DD}^{*2}\left[1+\left(\frac{\Gamma_\delta}{m_\delta}\right)^2 A_{\rm DD}\right]}, \tag{20}$$

for the potential one.

2.3 Short range correlations (case 3)

The idea here is to replace the kinetic part of the symmetry energy by that proposed in Ref. [24], where the authors have considered $\mathcal{S}^{\rm kin}$ as composed by a free gas model term added to a correction term $\Delta\mathcal{S}^{\rm kin}$ that takes into account short-range correlations between proton-neutron pairs in symmetric nuclear matter. Based on this procedure, we calculate the potential part of the symmetry energy as follows,

$$\mathcal{S}_{\rm i}^{\rm pot}(\rho)=\mathcal{S}_{\rm i}(\rho)-\mathcal{S}_{\rm SRC}^{\rm kin}(\rho), \tag{21}$$

where i = NL, DD. The expressions for the total symmetry energy $\mathcal{S}_{\rm i}(\rho)$ are given by the sum of Eqs. (12) and (14) for the NL model, or Eqs. (12) and (15) for the DD one, by using the formulae of case 1. Exactly the same expressions are found if case 2 is taken into account, i. e., if the sum of Eqs. (18) and (19) is performed for the NL model, or the sum of Eqs. (18) and (20) is considered for the DD model. Finally, the kinetic part of the symmetry energy for the present case analysis, $\mathcal{S}_{\rm SRC}^{\rm kin}(\rho)$, is taken from Ref. [24] as

$$\mathcal{S}_{\rm SRC}^{\rm kin}(\rho)=\left(2^{2/3}-1\right)\frac{3k_{\rm F}^2}{10M}-\Delta\mathcal{S}^{\rm kin}(\rho), \tag{22}$$

with

$$\Delta\mathcal{S}^{\rm kin}(\rho) = \frac{c_0 k_{\rm F}^{0\,2}}{2M\pi^2}\left[\lambda\left(\frac{\rho}{\rho_0}\right)^{1/3}-\frac{8}{5}\left(\frac{\rho}{\rho_0}\right)^{2/3}+\frac{3\rho}{5\lambda\rho_0}\right], \tag{23}$$

where the parameters c_0=4.48 and λ=2.75 are also taken from Ref. [24].

3 Results

Let's start by revisiting the analysis of the correlation between the symmetry energy $\mathcal{S}_0=\mathcal{S}(\rho_0)$ and its slope $L_0=L(\rho_0)$, both at saturation density, whose data are shown respectively in columns 1 and 4 in Tables 3, 4 and 5 (detail are given later) and are plotted in Fig. 1, where squares indicate the parametrizations which also satisfy the macroscopic stellar properties of $1.93\leqslant M_{\rm max}/M_\odot\leqslant 2.05$ from Refs. [3, 4]. This correlation

Table 3. Symmetry energy and its slope, with the respective kinetic and potential parts, all of them at $\rho=\rho_0$, obtained from the case 1 analysis for the CRMF parametrizations presenting $\Delta(\rho)\leqslant 15\%$ at a density range of $1\leqslant\rho/\rho_0\leqslant 4$ (see main text). The meanings of the symbols ✓ and □ are also defined in the text.

models	$\mathcal{S}_0$/MeV	$\mathcal{S}_0^{\rm kin}$/MeV	$\mathcal{S}_0^{\rm pot}$/MeV	L_0/MeV	$L_0^{\rm kin}$/MeV	$L_0^{\rm pot}$/MeV	γ_1
BKA20 ✓ □	32.24	16.58	15.66	75.38	48.47	26.91	0.57
BKA22 ✓ □	33.17	17.44	15.73	78.79	52.12	26.67	0.57
BKA24 ✓ □	34.19	17.54	16.65	84.80	52.09	32.70	0.65
BSR8 ✓	31.08	17.47	13.61	60.25	52.78	7.47	0.18
BSR9 ✓	31.61	17.57	14.05	63.89	52.41	11.49	0.27
BSR10 ✓	32.72	17.63	15.09	70.83	53.09	17.74	0.39
BSR11 ✓ □	33.69	17.47	16.22	78.78	51.89	26.89	0.55
BSR12 ✓	34.00	17.47	16.53	77.90	52.30	25.60	0.52
BSR15	30.97	17.33	13.65	61.79	49.34	12.45	0.30
BSR16	31.24	17.35	13.90	62.33	49.41	12.92	0.31
BSR17	31.98	17.38	14.60	67.44	49.50	17.93	0.41
BSR18	32.74	17.39	15.35	72.65	49.48	23.17	0.50
BSR19 □	33.78	17.40	16.38	79.47	49.52	29.96	0.61
BSR20 □	34.54	17.40	17.14	88.03	49.10	38.93	0.76
FSU-IV	31.43	17.45	13.98	52.16	49.72	2.44	0.06
FSUGold	32.56	17.45	15.11	60.44	49.72	10.72	0.24
FSUGold4	31.40	17.37	14.03	51.74	49.43	2.31	0.05
FSUGZ03 ✓	31.54	17.57	13.98	63.98	52.40	11.58	0.28
FSUGZ06	31.18	17.35	13.83	62.42	49.42	13.00	0.31
IU-FSU ✓	31.30	17.94	13.36	47.21	54.42	−7.21	−0.18
G2* ✓ □	30.39	16.61	13.77	69.68	46.31	23.37	0.57
Z271s5	31.84	13.82	18.02	53.57	32.55	21.02	0.39
Z271s6	31.20	13.82	17.38	47.81	32.55	15.25	0.29

has already been extensively investigated, for instance, in Refs. [19, 48–50] and only some of the points in Fig. 1 coincide with the overlap region of Fig. 2 in Ref. [48] (the gray band in our Fig. 1). This means that the accepted range of values in Ref. [2] is broader than the overlap of conditions shown in Ref. [48], namely, the overlap among constraints from nuclear masses, neutron skin thickness of Sn isotopes, dipole polarizability of ^{208}Pb, giant dipole resonances, isotope diffusion in heavy ion collisions, astrophysical observations, and neutron matter constraints.

We next obtain the γ values by using Eq. (10) for some CRMF parametrizations and then also compare our values with the ranges proposed in Refs. [24, 25]. In our analysis, we assume that the potential part of the symmetry energy can be written as in Eq. (8). Here, not all CRMF parametrizations are analyzed, but instead, only those in which the deviation defined by $\Delta(\rho)=|S^{\rm pot}_{\rm model}(\rho)-S^{\rm pot}_{\rm approx.}(\rho)|/S^{\rm pot}_{\rm model}(\rho)$ is less than a certain value, with $S^{\rm pot}_{\rm approx.}(\rho)=\mathcal{S}_0^{\rm pot}(\rho/\rho_0)^\gamma$, see Eq. (8). As for each case one has different values for γ, the function $S^{\rm pot}_{\rm approx.}(\rho)$ exhibits different density dependences for the same parametrization. Therefore, each studied case produces different values of $\Delta(\rho)$ for the same parametrization. Since experimental values of γ were extracted at suprasaturation density regime, we decided to investigate the values of $\Delta(\rho)$ at a range of $1\leqslant\rho/\rho_0\leqslant 4$, and define that only CRMF parametrizations, at this specific density range, presenting $\Delta\leqslant 15\%$, are taken into account in our study. By considering this analysis, we ensure a good agreement between the exact potential part of the symmetry energy, $S^{\rm pot}_{\rm exact}(\rho)$, of the CRMF parametrizations and the approximate form given in Eq. (8).

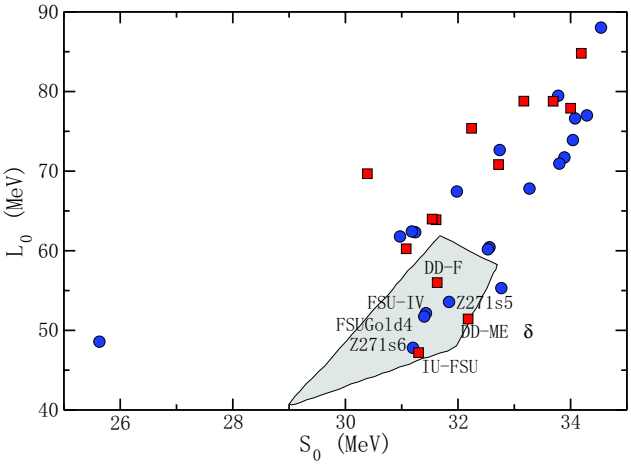

Fig. 1. (color online) Slope as a function of the symmetry energy for the CRMF models (all points). The gray band was extracted from Ref. [48]. The squares represent parametrizations which also satisfy the neutron star mass constraint of Refs. [3, 4].

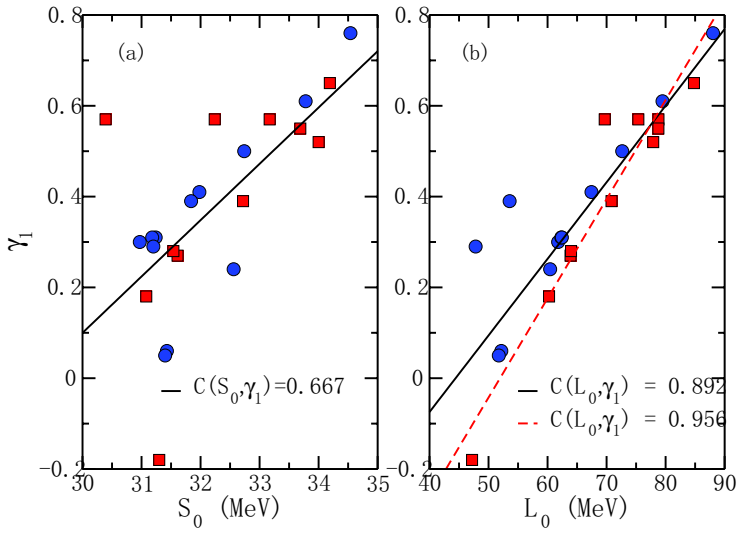

Fig. 2. (color online) γ_1 as a function of (a) symmetry energy, and (b) its slope, both at $\rho=\rho_0$, for the models displayed in Table 3 (all points). Squares represent parametrizations also satisfying the neutron star mass constraint of $1.93\leqslant M_{\rm max}/M_\odot\leqslant 2.05$ [3, 4]. The solid and dashed lines are fitting curves.

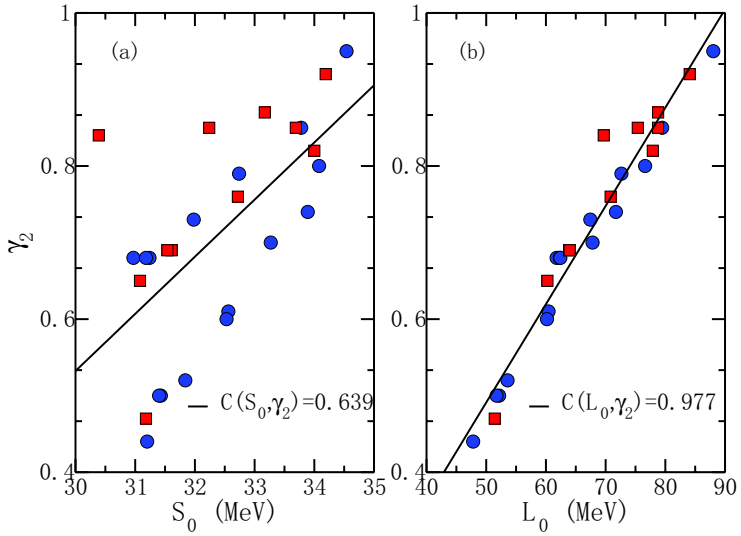

Fig. 3. (color online) γ_2 as a function of (a) symmetry energy, and (b) its slope, both at $\rho=\rho_0$, for the models of Table 4 (all points). Squares represent parametrizations also satisfying the neutron star mass constraint of $1.93\leqslant M_{\rm max}/M_\odot\leqslant 2.05$ [3, 4]. The solid lines are fitting curves.

As a further study, we analyse here the effect of the absence of the scalar interaction in the kinetic parts of the symmetry energy and its slope in the possible correlations of γ_2 with $\mathcal{S}_0$ and L_0. The results are shown in Fig. 3.

Our calculations were divided into the three different cases presented in Section 2. For each case, we construct a specific table where we use the symbol ✓ to mark those models in which the constraint $1.93\leqslant M_{\rm max}/M_\odot\leqslant 2.05$ for the maximum neutron star mass is also satisfied, the symbol □ to mark those parametrizations presenting the γ parameter in the range $\gamma=0.72\pm0.19$, and the symbol ☒ to identify parametrizations for which $\gamma=0.25\pm0.05$.

We next make a distinction between the two first cases (1 and 2) and case 3. For the last, one presented in Section 3.3, we have considered short-range correlations in the kinetic part of the symmetry energy. For cases 1 and 2 such an effect is not taken into account. For this reason, we compare in the next subsections the obtained values for the γ parameter in cases 1 and 2 only with the experimental range of $\gamma=0.72\pm0.19$, since this range was obtained without SRC effects, according to Ref. [25]. Furthermore, we name the parameters calculated from cases 1 and 2 respectively γ_1 and γ_2.

For case 3, the γ parameter obtained with SRC effects

is named γ_3. It is compared only with the experimental range γ=0.25±0.05 because this range was proposed in Ref. [24] with SRC included in the analysis.

3.1 Case 1

The γ values calculated from case 1 (γ_1) are presented in Table 3. From this table we notice only 7 parametrizations with γ_1 in the range γ=0.72±0.19. Furthermore, with data taken from columns 1, 4 and 7, we investigate possible correlations between γ_1 and the isovector quantities at the saturation density. The results are depicted in Fig. 2.

From Fig. 2(a), we observe a trend of linear correlation between γ_1 and $\mathcal{S}_0$. A quantitative measurement of such a finding can be given by calculation of the Pearson's correlation coefficient, defined as in Ref. [51]. Two different quantities, A and B, are strongly correlated within a linear relationship the closer the coefficient correlation $C(A,B)$ is to 1, or -1 in the case of a negative linear dependence. In the case of the $\mathcal{S}_0$ dependence of γ_1, we found $C(\mathcal{S}_0,\gamma_1)$=0.667.

By performing the same study in the $\gamma_1 \times L_0$ data, we noticed a better linear correlation than in the previous case, since the correlation coefficient resulted in $C(L_0,\gamma_1) = 0.892$, see Fig. 2(b). Moreover, if we restrict our analysis only to the points corresponding to the models in which the neutron star mass constraint is satisfied (squares), we see that the linear correlation is still stronger in comparison to the one exhibited with all points. The correlation coefficient for the square points in Fig. 2(b) is $C(L_0,\gamma_1)$=0.956.

3.2 Case 2

The γ_2 values calculated here are presented in Table 4. Since in this case we have prevented the kinetic part of the symmetry energy from having any influence on the effective mass, and as a consequence of the scalar meson effects, one can see here that $\mathcal{S}_0^{\rm kin}={k_{\rm F}^0}^2/(6E_{\rm F}^0)$ differs from each parametrization only due to the Fermi energy $E_{\rm F}^0=({k_{\rm F}^0}^2+M^2)^{1/2}$ at the saturation point. As $k_{\rm F}^0=(3\pi^2\rho_0/2)^{1/3}$, and as for nuclear mean-field models the saturation density is well established closely around the value of $\rho_0 = 0.15$ fm^{-3}, it becomes clear that the parametrizations analyzed according to Eqs. (18)-(20) present values of $\mathcal{S}_0^{\rm kin}$ in a very narrow band, as one can see from Table 4. For the same reason, the kinetic part of the symmetry energy slope, $L_0^{\rm kin}$, is also constrained to a small range. Also from Table 4, we see that for the case 2 analysis, a large number of parametrizations, namely, 20 of them, have γ_2 in the range γ=0.72±0.19.

Table 4. Symmetry energy and its slope, with the respective kinetic and potential parts, all of them at $\rho=\rho_0$, obtained from the case 2 analysis for the CRMF parametrizations presenting $\Delta(\rho)\leqslant 15\%$ at a density range of $1\leqslant\rho/\rho_0\leqslant 4$ (see main text). The meanings of the symbols ✓ and □ are also defined in the text.

models	$\mathcal{S}_0$/MeV	$\mathcal{S}_0^{\rm kin}$/MeV	$\mathcal{S}_0^{\rm pot}$/MeV	L_0/MeV	$L_0^{\rm kin}$/MeV	$L_0^{\rm pot}$/MeV	γ_2
BKA20 ✓ □	32.24	11.15	21.09	75.38	21.53	53.85	0.85
BKA22 ✓ □	33.17	11.21	21.96	78.79	21.64	57.15	0.87
BKA24 ✓	34.19	11.20	22.99	84.80	21.63	63.17	0.92
BSR8 ✓ □	31.08	11.19	19.88	60.25	21.62	38.64	0.65
BSR9 ✓ □	31.61	11.21	20.40	63.89	21.65	42.24	0.69
BSR10 ✓ □	32.72	11.22	21.50	70.83	21.66	49.17	0.76
BSR11 ✓ □	33.69	11.19	22.50	78.78	21.60	57.18	0.85
BSR12 ✓ □	34.00	11.22	22.78	77.90	21.66	56.24	0.82
BSR15 □	30.97	11.13	19.85	61.79	21.49	40.30	0.68
BSR16 □	31.24	11.13	20.11	62.33	21.50	40.83	0.68
BSR17 □	31.98	11.17	20.81	67.44	21.57	45.87	0.73
BSR18 □	32.74	11.14	21.59	72.65	21.52	51.13	0.79
BSR19 □	33.78	11.19	22.60	79.47	21.60	57.87	0.85
BSR20	34.54	11.15	23.38	88.03	21.54	66.48	0.95
FSU-III □	33.89	11.26	22.64	71.72	21.73	49.99	0.74
FSU-IV	31.43	11.26	20.17	52.16	21.73	30.43	0.50
FSUGold4	31.40	11.22	20.18	51.74	21.66	30.07	0.50
FSUGZ03 ✓ □	31.54	11.21	20.33	63.98	21.65	42.33	0.69
FSUGZ06 □	31.18	11.14	20.04	62.42	21.51	40.92	0.68
G2* ✓ □	30.39	11.52	18.87	69.68	22.22	47.46	0.84
Z271s2 □	34.08	11.27	22.81	76.62	21.75	54.87	0.80
Z271s3 □	33.27	11.27	22.00	67.81	21.75	46.05	0.70
Z271s4 □	32.53	11.27	21.26	60.18	21.75	38.43	0.60
Z271s5	31.84	11.27	20.57	53.57	21.75	31.82	0.52
Z271s6	31.20	11.27	19.93	47.81	21.75	26.05	0.44
DD-MEδ ✓	32.18	11.44	20.74	51.43	22.08	29.35	0.47

Table 5. Symmetry energy and its slope, with the respective kinetic and potential parts, all of them at $\rho=\rho_0$, obtained from the case 3 analysis for the CRMF parametrizations presenting $\Delta(\rho)\leqslant 15\%$ at a density range of $1\leqslant\rho/\rho_0\leqslant 4$ (see main text). The meanings of the symbols ✓ and ☒ are also defined in the text.

models	$\mathcal{S}_0$/MeV	$\mathcal{S}^{\rm kin}_{\rm SRC,0}$/MeV	$\mathcal{S}^{\rm pot}_0$/MeV	L_0/MeV	$L^{\rm kin}_0$/MeV	$L^{\rm pot}_0$/MeV	γ_3
BKA20 ✓	32.24	−9.31	41.55	75.38	21.21	54.16	0.43
BKA22 ✓	33.17	−9.36	42.53	78.79	21.33	57.46	0.45
BKA24 ✓	34.19	−9.35	43.54	84.80	21.31	63.48	0.49
BSR8 ✓	31.08	−9.35	40.43	60.25	21.30	38.95	0.32
BSR9 ✓	31.61	−9.37	40.98	63.89	21.34	42.55	0.35
BSR10 ✓	32.72	−9.37	42.09	70.83	21.35	49.48	0.39
BSR11 ✓	33.69	−9.34	43.03	78.78	21.29	57.49	0.44
BSR12 ✓	34.00	−9.37	43.37	77.90	21.35	56.55	0.43
BSR15	30.97	−9.29	40.26	61.79	21.17	40.62	0.34
BSR16	31.24	−9.30	40.54	62.33	21.18	41.15	0.34
BSR17	31.98	−9.33	41.31	67.44	21.25	46.18	0.37
BSR18	32.74	−9.31	42.04	72.65	21.20	51.45	0.41
BSR19	33.78	−9.34	43.13	79.47	21.29	58.19	0.45
BSR20	34.54	−9.31	43.85	88.03	21.22	66.80	0.51
FSU-III	33.89	−9.40	43.30	71.72	21.43	50.30	0.39
FSU-IV ☒	31.43	−9.40	40.83	52.16	21.43	30.73	0.25
FSUGold	32.56	−9.40	41.96	60.44	21.43	39.01	0.31
FSUGold4 ☒	31.40	−9.37	40.77	51.74	21.35	30.38	0.25
FSUGZ03 ✓	31.54	−9.37	40.91	63.98	21.34	42.64	0.35
FSUGZ06	31.18	−9.30	40.48	62.42	21.19	41.24	0.34
IU-FSU ✓ ☒	31.30	−9.67	40.97	47.21	22.04	25.17	0.20
G2* ✓	30.39	−9.63	40.02	69.68	21.94	47.74	0.40
Z271s2	34.08	−9.41	43.49	76.62	21.45	55.18	0.42
Z271s3	33.27	−9.41	42.68	67.81	21.45	46.36	0.36
Z271s4	32.53	−9.41	41.94	60.18	21.45	38.74	0.31
Z271s5 ☒	31.84	−9.41	41.25	53.57	21.45	32.12	0.26
Z271s6 ☒	31.20	−9.41	40.61	47.81	21.45	26.36	0.22
DD-MEδ ✓ ☒	32.18	−9.56	41.75	51.43	21.79	29.64	0.24

From this figure one can see that the trend of linear correlation between γ_2 and $\mathcal{S}_0$ is worse when compared with case 1, since in case 2 one has $C(\mathcal{S}_0,\gamma_2)=0.639$. However, we see that the linear correlation $\gamma_2\times L_0$ is favored when the kinetic parts of the symmetry energy and its slope are free from the scalar interaction effects. The correlation coefficient in this case is $C(L_0,\gamma_2)=0.977$, a higher value than the corresponding one of the previous case, namely, $C(L_0,\gamma_1)=0.892$.

3.3 Case 3

The use of Eqs. (21)-(23) along with Eq. (7), all of them evaluated at $\rho=\rho_0$, allows the calculation of γ_3 from the definition given in Eq. (10). The results are presented in Table 5. In our procedure, only the sum of the kinetic and potential parts of the symmetry energy matters. This sum does not change, and we extract the potential part by subtracting from the total (exact) value, the kinetic part with SRC included, as indicated in Eq. (21).

From Table 5 we see that $\mathcal{S}^{\rm kin}_{\rm SRC,0}$ has a negative value around −9.3 MeV for all parametrizations. Such a feature is a direct consequence of the short-range correlations between proton-neutron pairs in symmetric nuclear matter introduced in Ref. [24], that produced the expressions presented in Eqs. (22)-(23). Such a negative value for $\mathcal{S}^{\rm kin}_0$ of the CRMF parametrizations is indeed consistent with the range of -10 ± 7.5 MeV found by the authors [24] through the analysis of data from free proton-to-neutron ratios measured in intermediate energy nucleus-nucleus collisions.

We also see from Table 5 that the introduction of short-range correlations produces 6 parametrizations with γ_3 in the range of $\gamma=0.25\pm0.05$.

In Fig. 4, we also investigate the γ_3 correlations. It is clear from this figure that the linear dependence between γ_3 and the isovector bulk parameters is still more favored when the short-range correlations are included in the CRMF parametrizations. The correlation coefficients obtained in this case are the closest to the unity, namely, $C(\mathcal{S}_0,\gamma_3)=0.689$ and $C(L_0,\gamma_3)=0.994$ in comparison with the respective quantities regarding the cases 1 and 2.

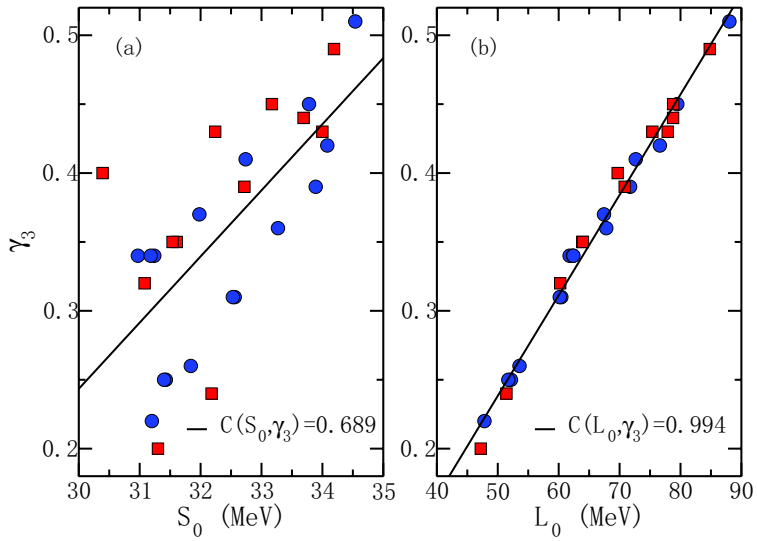

Fig. 4. (color online) γ_3 as a function of (a) symmetry energy, and (b) its slope, both at $\rho=\rho_0$, for the models of Table 5 (all points). Squares represent parametrizations also satisfying the neutron star mass constraint of $1.93\leqslant M_{\rm max}/M_\odot\leqslant 2.05$ [3, 4]. The solid lines are fitting curves.

3.4 Comments about the results

Regarding the correlations found mainly between γ and L_0, we remark that such a result is not trivial, and the reason can be given from an analysis of Eq. (10). From such an equation we can write:

$$\gamma=\alpha L_0+\beta, \tag{24}$$

with $\alpha=1/(3S_0^{\rm pot})$ and $\beta=-L_0^{\rm kin}/(3S_0^{\rm pot})$, i. e., a linear correlation between γ and L_0 is obtained if α and β are (ideally) constant numbers. In our study, we investigate whether $L_0^{\rm kin}$ and $S_0^{\rm pot}$ are close enough to constants for the sets of parametrization studied in each case. If this is the case, the variations $\Delta\alpha$ and $\Delta\beta$ are close to zero. Since for each case studied we have the highest and lowest values of $S_0^{\rm pot}$ and $L_0^{\rm kin}$, it is possible to calculate $\Delta\alpha=\frac{1}{3(S_0^{\rm pot})_{\rm high}}-\frac{1}{3(S_0^{\rm pot})_{\rm low}}$, and $\Delta\beta=-\frac{(L_0^{\rm kin})_{\rm high}}{3(S_0^{\rm pot})_{\rm high}}+\frac{(L_0^{\rm kin})_{\rm low}}{3(S_0^{\rm pot})_{\rm low}}$. The absolute values of such calculations are shown in Table 6, and as one can see, $\Delta\alpha$ and $\Delta\beta$ are decreasing quantities if we analyse such numbers from case 1 to 3. These behaviors explain the increasing coefficient correlation shown in Figs. 2 to 4.

Table 6. Absolute values of $\Delta\alpha$ and $\Delta\beta$, calculated for the three different cases analyzed.

case	$\lvert\Delta\alpha\rvert$/MeV^{-1}	$\lvert\Delta\beta\rvert$
1	0.0064	0.756
2	0.0034	0.085
3	0.0007	0.022

This result is a consequence of the data previously presented in Tables 3, 4 and 5. From these tables, one can see that the values of $L_0^{\rm kin}$ and $S_0^{\rm pot}$ are closer to a constant value in case 3 than in case 2. Also, these values are closer to a certain constant value in case 2 than in case 1.

One can see from such a table that the closer results are obtained for the cases in which the scalar attractive interaction is not taken into account in the kinetic part of the symmetry energy, i. e., cases 2 and 3, the latter being the case in which $\Delta\alpha$ and $\Delta\beta$ are closer to zero.

As a direct application of this specific correlation, we also investigate whether γ_1, γ_2, and γ_3 obtained from the CRMF parametrizations in the three different cases studied and always calculated for symmetric nuclear matter, also correlate with neutron star radii. The motivation for such a study comes from the results presented in Ref. [52], in which the authors found that for a class of 42 relativistic and Skyrme parametrizations, L_0 linearly depends on $R_{1.0}$ and $R_{1.4}$, namely, the radii of neutron stars presenting $M_{\rm star}=M_\odot$ and $1.4M_\odot$, respectively. The $R_{1.0}$ and $R_{1.4}$ dependence of γ_1, γ_2, γ_3 related to those CRMF parametrizations analyzed here is shown in Fig. 5. In order to obtain stellar macroscopic properties, the same CRMF parametrizations are used, but now the models are subject to matter neutrality and β-equilibrium.

In order to generate the neutron star radii, we have joined the hadronic matter EoS from the CRMF parametrizations with those for electrons and muons. After that, the conditions of charge neutrality and chemical equilibrium were taken into account and the Baym-Pethick-Sutherland (BPS) equation of state [53] for low densities was added to the EoS for hadrons and leptons. The resulting EoS was used as input to the Tolman-Oppenheimer-Volkoff equations [54]. We refer the reader to Ref. [55], for instance, for details regarding such calculations.

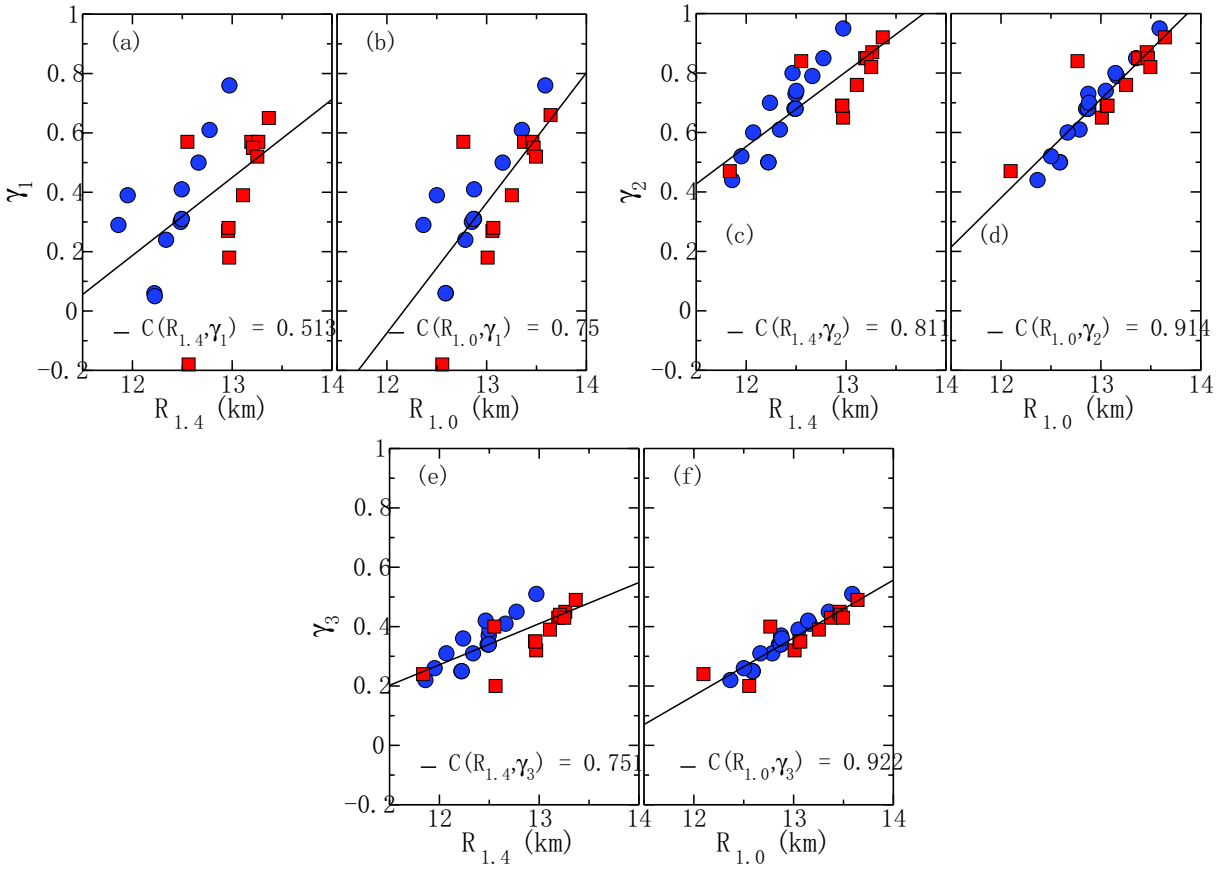

Fig. 5. (color online) γ_1, γ_2, and γ_3 as a function of the $R_{1.0}$ and $R_{1.4}$ neutron star radii for the CRMF parametrizations (all points). Squares represent parametrizations also satisfying the constraint of $1.93 \leqslant M_{\max}/M_{\odot} \leqslant 2.05$ [3, 4].

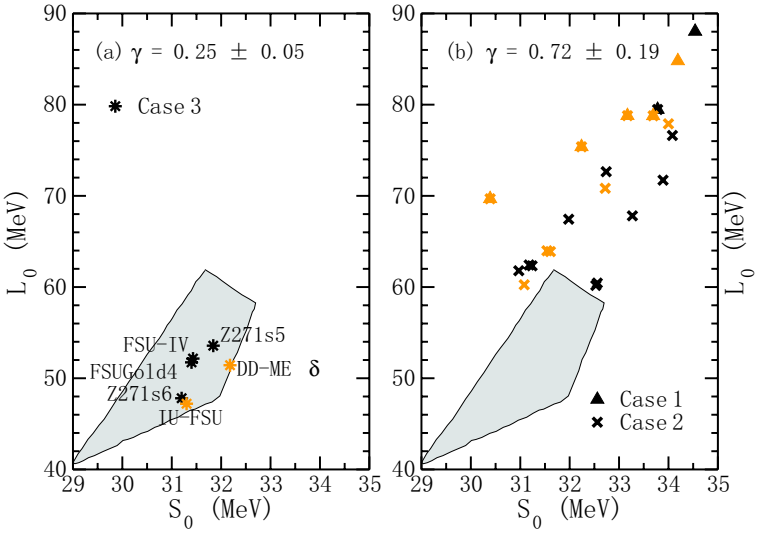

Fig. 6. (color online) Slope as a function of the symmetry energy for the models that produce the (a) lower and (b) higher γ ranges discussed in the last section. The gray band was extracted from Ref. [48]. Orange points represent those parametrizations in which the neutron star mass constraint of $1.93 \leqslant M_{\max}/M_{\odot} \leqslant 2.05$ [3, 4] is verified.

From Fig. 5, we can conclude that the CRMF parametrizations also present a linear behavior concerning γ_1, γ_2, γ_3 and the neutron star radii. This result is entirely compatible with the findings of Ref. [52]. In that paper, a linear correlation between L_0 and the radii was found, and since in our study we have found a linear dependence for γ_1, γ_2, γ_3 and L_0, according to Eq. (24), a direct consequence is the linear behavior described in Fig. 5. Also as in Ref. [52], the correlations are stronger for the $R_{1.0}$ neutron star radius as the correlation coefficients $C(R_{1.0},\gamma)$ point out. Finally, as observed in all the investigations, the linear dependence is intensified in cases 2 and 3, in which the effects of the scalar interaction are absent from the kinetic part of the symmetry energy.

Another point concerns the gray band in Fig. 1 for the CRMF models in the different cases studied. We start by redrawing, as shown in Fig. 6, such a figure for the different models that reproduce γ=0.25±0.05 (Fig. 6(a)) and γ=0.72±0.19 (Fig. 6(b)).

The CRMF parametrizations for which we have obtained the γ parameters from case 3 are more compatible with the gray band proposed in Ref. [48], i. e., the short-range correlations effects induce the CRMF parametrizations to present the γ parameter inside the range of γ=0.25±0.05, simultaneously being consistent with the overlap conditions of Ref. [48] obtained from many experimental and observational data. For such a case, 6 parametrizations are inside the overlap band, namely, IU-FSU, FSU-IV, FSUGold4, Z271s5, Z271s6, and DD-MEδ, with 2 of them, IU-FSU and DD-MEδ, also satisfying the neutron star mass constraint of $1.93\leqslant M_{\max}/M_{\odot}\leqslant 2.05$ [3, 4] and two of them, Z271s5 and Z271s6 yielding critical parameters close to the existing proposition of experimental values, according to the findings of Ref. [5].

4 Summary

In summary, our calculations have shown that, independently of the choice made to obtain the γ values (case 1, 2 or 3) for the CRMF models, a trend of linear correlation is observed between γ_1, γ_2, γ_3 and $\mathcal{S}_0$, and a clearer linear relationship is established regarding γ_1, γ_2, γ_3 and the slope of the symmetry energy at the saturation density, L_0. In cases 2 and 3, the last correlation is still more pronounced. Such an effect arises due to the absence of the attractive interaction in the kinetic part of the symmetry energy. Furthermore, the short-range correlations introduced in the case 3 analysis intensify the linear L_0 dependence of γ_3, as seen in Fig. 4(b). These results can be used to determine other linear correlations of γ_1, γ_2, γ_3 and the neutron star radii of $R_{1.0}$ and $R_{1.4}$, as displayed in Fig. 5. Finally, specifically for case 3, two specific parametrizations, namely, IU-FSU and DD-MEδ are shown to be compatible with the range of γ=0.25±0.05 [24], and simultaneously consistent with the neutron star mass constraint of Refs. [3, 4], and other two, Z271s5 and Z271s6, simultaneously compatible with the range of γ=0.25±0.05 [24] and with probable critical parameters experimental values [5]. The four parametrizations are consistent with the overlap band for the $L_0\times\mathcal{S}_0$ region described in Ref. [48], see Fig. 6.

As a final remark, we remind the reader that we have only analyzed symmetric matter in this study **for the calculation of the γ values**, but the potential difference for neutrons and protons in neutron-rich matter and their density dependence, for instance, can also be calculated. However, the results cannot be compared with the existing γ values. Furthermore, if we also want to investigate the momentum dependence in asymmetric matter, single particle potentials, which are different for neutrons and protons, have to be taken into account, see Ref. [56, 57]. To obtain this kind of dependence, one would need either a theory that uses non-local interactions or a Thomas-Fermi calculation, and both approaches are out of the scope of the present work.

E. P. thanks the Brazilian Physical Society and the organizers of the XXXVIII RTFNB (nuclear physics annual meeting) for the invitation in 2015, when this collaboration started. This work is a part of the project INCT-FNA Proc. No. 464898/2014-5, was partially supported by CNPq (Brazil) under grants 300602/2009-0 (DPM) and 306786/2014-1 (OL).

References

1 M. Dutra, O. Lourenço, S. S. Avancini, B. V. Carlson, A. Delfino, D. P. Menezes, C. Providência, S. Typel, and J. R. Stone, Phys. Rev. C, **90**: 055203 (2014)
2 M. Dutra, O. Lourenço, and D. P. Menezes, Phys. Rev. C, **93**: 025806 (2016); Phys. Rev. C, **94**: 049901(E) (2016)
3 P. B. Demorest, T. Pennucci, S. M. Ransom, M. S. E. Roberts, and J. W. T. Hessels, Nature, **467**: 1081 (2010)
4 J. Antoniadis, P. C. C. Freire, N. Wex et al, Science, **340**: 448 (2013)
5 O. Lourenço, M. Dutra, and D. P. Menezes, Phys. Rev. C, **95**: 065212 (2017)
6 G. Bertsch and P. J. Siemens, Phys. Lett. B, **126**: 9 (1983); J. Margueron and P. Chomaz, Phys. Rev. C, **67**: 041602 (2003); C. Ducoin, Ph. Chomaz, and F. Gulminelli, Nucl. Phys. A, **771**: 68 (2006)
7 H. Müller and B. D. Serot, Phys. Rev. C, **52**: 2072 (1995)
8 Ph. Chomaz, C. Colonna, and J. Randrup, Phys. Rep., **389**: 263 (2004)
9 J. B. Silva, O. Lourenço, A. Delfino, J. S. Sá Martins, and M. Dutra, Phys. Lett. B, **664** 246, (2008)
10 V. Vovchenko, D. V. Anchishkin, and M. I. Gorenstein, Phys.

Rev. C, **91**: 064314 (2015)
11 V. Vovchenko, D. V. Anchishkin, M. I. Gorenstein, and R. V. Poberezhnyuk, Phys. Rev. C, **92**: 054901 (2015)
12 V. Vovchenko, Phys. Rev. C, **96**: 015206 (2017)
13 M. Baldo, G. F. Burgio, Prog. Part. Nucl. Phys., **91**: 203 (2016)
14 C. J. Horowitz and J. Piekarewicz, Phys. Rev. Lett., **86**: 5647 (2001)
15 S. S. Avancini, J. R. Marinelli, D. P. Menezes, M. M. W. Moraes, and C. Providência, Phys. Rev. C, **75**: 055805 (2007)
16 L. L. Lopes and D. P. Menezes, Braz. Jour. Phys., **44**: 774 (2014)
17 R. Cavagnoli, D. P. Menezes, and C. Providência, Phys. Rev. C, **84**: 065810 (2011)
18 P. K. Panda, A. M. S. Santos, D. P. Menezes, and C. Providência, Phys. Rev. C, **85**: 055802 (2012)
19 C. Providência et al, Eur. Phys. J. A, **50**: 44 (2014)
20 H. Pais, A. Sulaksono, B. K. Agrawal, and C. Providência, Phys. Rev. C, **93**: 045802 (2016)
21 S. S. Avancini, L. Brito, J. R. Marinelli, D. P. Menezes, M. M. W. de Moraes, C. Providência, and A. M. Santos, Phys. Rev. C, **79**: 035804 (2009)
22 M. B. Tsang, Yingxun Zhang, P. Danielewicz, M. Famiano, Zhuxia Li, W. G. Lynch, and A. W. Steiner, Phys. Rev. Lett., **102**: 122701 (2009)
23 Andrew W. Steiner, James M. Lattimer, and Edward F. Brown, Astrophys J., **722**: 33 (2010)
24 Or Hen, Bao-An Li, Wen-Jun Guo, L. B. Weinstein, and Eliezer Piasetzky, Phys. Rev. C, **91**: 025803 (2015)
25 P. Russotto et al, Phys. Rev. C, **94**: 034608 (2016)
26 J. Meng, H. Toki, S. G. Zhou, S. Q. Zhang, W. H. Long, and L. S. Geng, Prog. Part. Nucl. Phys., **57**: 470 (2006)
27 B. K. Agrawal, Phys. Rev. C, **81**: 034323 (2010)
28 S. K. Dhiman, R. Kumar, and B. K. Agrawal, Phys. Rev. C, **76**: 045801 (2007)
29 B.-J. Cai and L.-W. Chen, Phys. Rev. C, **85**: 024302 (2012)
30 B. G. Todd-Rutel and J. Piekarewicz, Phys. Rev. Lett., **95**: 122501 (2005)
31 J. Piekarewicz and S. P. Weppner, Nucl. Phys. A, **778**: 10 (2006)
32 R. Kumar, B. K. Agrawal, and S. K. Dhiman, Phys. Rev. C, **74**: 034323 (2006)
33 A. Sulaksono and T. Mart, Phys. Rev. C, **74**: 045806 (2006)
34 F. J. Fattoyev, C. J. Horowitz, J. Piekarewicz, and G. Shen, Phys. Rev. C, **82**: 055803 (2010)
35 C. J. Horowitz and J. Piekarewicz, Phys. Rev. C, **66**: 055803 (2002)
36 T. Klähn et al, Phys. Rev. C, **74**: 035802 (2006)
37 S. Typel and H. H. Wolter, Nucl. Phys. A, **656**: 331 (1999)
38 T. Gaitanos, M. Di Toro, S. Typel, V. Baran, C. Fuchs, V. Greco, and H. H. Wolter, Nucl. Phys. A, **732**: 24 (2004)
39 X. Roca-Maza, X. Viñas, M. Centelles, P. Ring, and P. Schuck, Phys. Rev. C, **84**: 054309 (2011)
40 J. J. Rusnak and R. J. Furnstahl, Nucl. Phys. A, **627**: 495 (1997)
41 B. A. Nikolaus, T. Hoch, and D. G. Madland, Phys. Rev. C, **46**: 1757 (1992)
42 D. G Madland, T. J Bürvenich, J. A Maruhn, and P.-G Reinhard, Nucl. Phys. A **741**: 52 (2004)
43 O. Lourenço, M. Dutra, A. Delfino, and R. L. P. G. Amaral, Int. Jour. Mod. Phys. E, **16**: 3037 (2007)
44 T. Niksic, D. Vretenar, and P. Ring, Prog. in Part. and Nucl. Phys., **66**: 519 (2011)
45 R. Subedi et al, Science, **320**: 1476 (2008)
46 O. Hen et al, Science, **346**: 614 (2014)
47 O. Hen, G. A. Miller, E. Piasetzky, and L. B. Weinstein, to apear in Rev. Mod. Phys., (2017)
48 J. M. Lattimer and Y. Lim, Astrophys. J., **51**: 771 (2013)
49 *Neutron Star Crust*: editors Carlos Bertulani and Jorge Pieckarewicz, Nova Science Publishers, 2012, New York
50 B. M. Santos, M. Dutra, O. Lourenço, and A. Delfino, Phys. Rev. C, **90**: 035203 (2014); **92**: 015210 (2015)
51 S. Brandt, *Data Analysis: Statistical and Computational Methods for Scientists and Engineers*: 4th ed. (Springer, New York, 2014)
52 N. Alam, B. K. Agrawal, M. Fortin, H. Pais, C. Providência, Ad. R. Raduta, and A. Sulaksono, Phys. Rev. C, **94**: 052801(R) (2016)
53 G. Baym, C. Pethick, and P. Sutherland, Astrophys. J., **170**: 299 (1971)
54 J. R. Oppenheimer, G. M. Volkoff, Phys. Rev., **33**: 374 (1939)
55 N. K. Glendenning, *Compact Stars*: 2nd ed. (Springer, New York, 2000); P. Haensel, A. Y. Potekhin, and D. G. Yakovlev, *Neutron Stars, Equation of State and Structure* (Springer, New York, 2006)
56 Bao-An Li, W. Udo Schröder (Eds.), *Isospin Physics in Heavy-Ion Collisions at Intermediate Energies*: Nova Science Publishers, Huntington, NY, 2001
57 Bao-An Li, Champak B. Das, Subal Das Gupta, and Charles Gale, Nuc. Phys. A, **735**: 563 (2004)